nature chemical biology

ARTICLES

https://doi.org/10.1038/s41589-019-0407-2

Computational design of G Protein-Coupled Receptor allosteric signal transductions

Kuang-Yui Michael Chen[1,2,5,6], Daniel Keri[1,6] and Patrick Barth[1,2,3,4*]

Membrane receptors sense and transduce extracellular stimuli into intracellular signaling responses but the molecular underpinnings remain poorly understood. We report a computational approach for designing protein allosteric signaling functions. By combining molecular dynamics simulations and design calculations, the method engineers amino-acid 'microswitches' at allosteric sites that modulate receptor stability or long-range coupling, to reprogram specific signaling properties. We designed 36 dopamine D2 receptor variants, whose constitutive and ligand-induced signaling agreed well with our predictions, repurposed the D2 receptor into a serotonin biosensor and predicted the signaling effects of more than 100 known G-protein-coupled receptor (GPCR) mutations. Our results reveal the existence of distinct classes of allosteric microswitches and pathways that define an unforeseen molecular mechanism of regulation and evolution of GPCR signaling. Our approach enables the rational design of allosteric receptors with enhanced stability and function to facilitate structural characterization, and reprogram cellular signaling in synthetic biology and cell engineering applications.

Allostery enables long-range communication between distant sites on a molecule, and underlies the regulation of a wide range of biomolecular functions, but its biophysical underpinnings remain poorly understood. Allosteric communications are thought to be primarily mediated by intraprotein networks of coupled residues (that is, allosteric residues) physically connecting distant protein regions[1,2]. Long-range structural couplings promote long-distance communication through the propagation of even small changes in local structure and dynamics[3–6]. Coupled allosteric residues display correlated motions and can be identified by molecular dynamics (MD) simulations[7–9]. Allosteric sites are functionally very sensitive to mutations[10], enabling the modulation of protein function even between closely related protein sequences[11]. Hence, predicting how receptor sequences and structures encode specific allosteric responses remains particularly challenging.

GPCRs[12] represent the largest family of membrane-embedded allosteric proteins that receive external stimuli in the form of light, hormones, odorants, neurotransmitters or peptides; and allosterically transduce these stimuli across the membrane to initiate intracellular signaling pathways[13–15]. In the largest family (class A) of GPCRs, signal transductions involve a few highly conserved allosteric sites (called microswitches) that undergo consensus structural changes triggering receptor activation[16–18]. However, these allosteric sites are not in direct contact and their conserved mechanism of action does not explain the large diversity of allosteric signal transduction responses displayed by class A GPCRs[19,20]. How the conserved microswitches are physically connected throughout the receptor structure and define the allosteric pathways that control selective signal transductions remains poorly understood.

Better understanding and engineering allostery in receptors would greatly benefit not only the study of receptor structure, function and pharmacology but also the design of new biosensing receptors for synthetic and cell biology applications. Empirical approaches for screening stabilized mutants have been developed to facilitate structure determination[21]. However, the thermostabilized receptors often no longer exhibited the native ligand-induced signal transduction responses, highlighting the challenges in understanding the determinants regulating receptor stability and function[22–24]. Protein engineering techniques that reprogram conformational stability and long-range allosteric coupling have not yet been reported.

Here, we developed a computational protein design approach linking protein conformational stability, dynamics, ligand binding and allosteric regulation of protein activity to rationally design receptors with reprogrammed signaling activities. We validated this approach by engineering the GPCR, dopamine D2 receptor (D2), whose active state structure is unknown, with reprogrammed constitutive and ligand-induced G protein activation. We report designed D2 variants with considerably enhanced potency and signaling responses to the native ligand agonist dopamine and the non-native ligand serotonin. We also predicted the effects of more than 100 known mutations on the signaling activities of several GPCRs. The approach is general and should prove useful for designing new membrane receptor biosensors. Last, our study revealed new insights into the role of allosteric pathways in the regulation and evolution of GPCR signaling functions.

Results

Computational design framework of GPCR signaling. To implement our approach, we took advantage of the rich experimental structural information on GPCRs, the prediction of allosteric residues by MD simulations and theoretical allosteric models linking protein conformational stability, ligand binding and long-range structural coupling to the regulation of receptor activation. Using this knowledge, we developed a general design approach combining protein structure, dynamics and allostery to engineer protein signaling functions described in detail below.

[1]Swiss Federal Institute of Technology (EPFL), Institute of Bioengineering, Lausanne, Switzerland. [2]Verna and Marrs McLean Department of Biochemistry and Molecular Biology, Baylor College of Medicine, Houston, TX, USA. [3]Department of Pharmacology, Baylor College of Medicine, Houston, TX, USA. [4]Structural and Computational Biology and Molecular Biophysics Graduate Program, Baylor College of Medicine, Houston, TX, USA. [5]Present address: Department of Cell Biology and Human Anatomy, University of California at Davis, Davis, CA, USA. [6]These authors contributed equally: Kuang-Yui Michael Chen, Daniel Keri. *e-mail: patrick.barth@epfl.ch

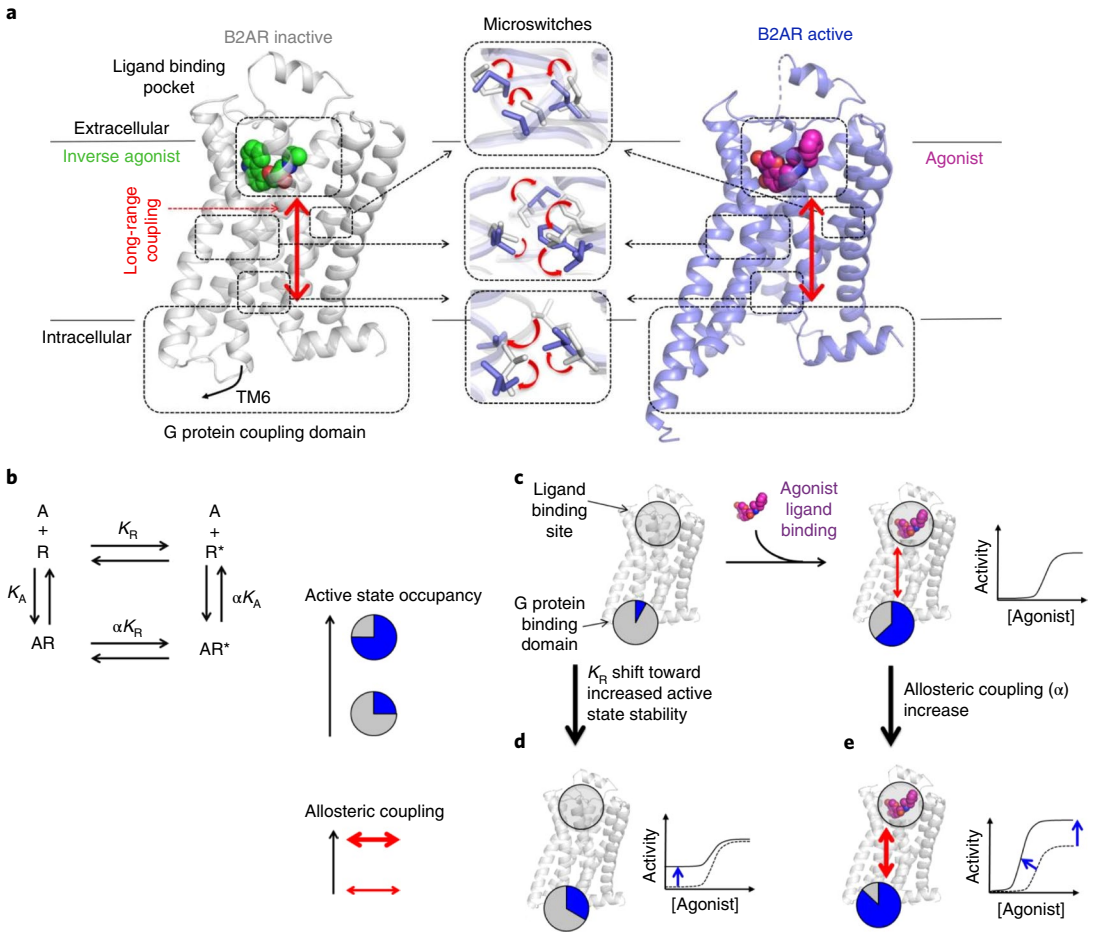

Fig. 1 | Rational design of GPCR allosteric regulation. a, Left and right, B2AR inactive (gray) and active (blue) state X-ray structures bound to inverse agonist and agonist ligands, respectively. The red arrow depicts schematically the structural coupling connecting the extracellular ligand binding pocket and the intracellular G protein binding domain. Middle, amino-acid microswitches are highlighted for three local TM regions with their movements indicated by curved red arrows. **b**, ATSM describing the regulation of receptor activity by ligand binding. **c**–**e**, Effects of ligand binding, protein stability and allosteric coupling on receptor activity according to the ATSM. **c**, Effects of agonist ligand binding on receptor activity. Inactive and active receptor G protein binding site conformation occupancies are indicated in gray and blue pie fractions, respectively. Left, in the absence of an agonist, the G protein binding site mostly occupies the inactive conformation. Right, the agonist-bound ligand site preferentially couples to the active conformation of the G protein binding site, increasing active state occupancy and enhancing receptor intracellular activity. **d**, Increasing the stability of the active relative to that of the inactive state conformation (that is, increase K_R) enhances the receptor activity even in absence of ligand (that is, constitutive). **e**, Increasing the allosteric coupling of the ligand agonist enhances the stabilization by the ligand of the G protein binding site active conformation and the intracellular response (that is, activity) of the receptor to agonist binding. In this example, K_R and therefore the receptor constitutive activity remain unchanged.

GPCR structures are composed of three main regions: the extracellular ligand binding pocket, the intracellular G protein binding domain and the 'transmission' transmembrane (TM) region that connects the two binding regions and allows them to communicate[13,14] (Fig. 1a). GPCRs typically switch from inactive to active state conformations on activating agonist ligand and G protein binding. Receptor activation involves large intracellular reorientations of transmembrane helices (TMH) TMH6 and TMH7 and smaller scale movements of individual amino-acids (we define these residues as microswitches) across the entire TM domain (Fig. 1a). As identified by MD simulations, many microswitches display correlated motions, are organized in sparse allosteric networks that couple the extracellular and intracellular domains of the receptor across long-distance[7–9], and are defined as allosteric microswitches in our study. By changing conformations during receptor activation, microswitches form new sets of contacts in distinct receptor functional states. Therefore, microswitches can selectively fine-tune the stability or the long-range structural coupling within each receptor conformation, which can be used to design protein signaling functions as outlined below.

While protein allostery can involve multiple functional conformations, the regulation of protein signaling can be described, to a first approximation, using the allosteric two-state model (ATSM) that provides a theoretical framework linking protein stability, ligand binding and allosteric coupling to the receptor activity[13] (Fig. 1b–e and Supplementary Fig. 1). In this model, the receptor occupies two main functional states: an inactive (R) and an active (R*) state in which the ligand and G protein binding site conformations are the most coupled. In absence of ligand, most native GPCRs primarily occupy the more stable inactive state (that is, $K_R < 1$, where the apo equilibrium constant, $K_R = [R^*]/[R]$, see Fig. 1b) and therefore display low constitutive activity[25] (Fig. 1c, left). Extracellular ligands often display different affinities for the inactive and active conformations of the ligand binding site and can therefore regulate receptor function by stabilizing distinct receptor states[25]. The ability of a ligand to selectively stabilize a receptor state is at the origin of

the allosteric effect and measured by the allosteric coupling alpha (that is, α, where $\alpha KR = [AR^*]/[AR]$, see Fig. 1b), which is related to the structural coupling as described below and in the methods. For example, agonists preferentially interact with the ligand binding active conformation (that is, $\alpha > 1$) that is most coupled to the active conformation of the G protein binding site. Consequently, agonist binding preferentially stabilizes the receptor active state, leading to increased receptor activity and intracellular signaling (Fig. 1c, right). The reverse scenario occurs with inverse agonists (Supplementary Fig. 1).

According to the ATSM, receptor activity can be modulated through three distinct mechanisms (Fig. 1d–e and Supplementary Fig. 1d–k). (1) Increasing the stability of the active compared to that of the inactive ligand-free structures (that is, increase K_R) will enhance the receptor activity even in the absence of ligand agonist (that is, constitutive activity) (Fig. 1d). (2) Modifying the allosteric coupling (α) of a ligand will shift the receptor response to ligand binding. As demonstrated previously[26] and herein (Methods), this can be achieved by altering the long-range structural coupling between the ligand and G protein binding sites in selective receptor conformations. For example, optimizing the structural coupling of the agonist-bound ligand site with the active but not with the inactive conformation of the G protein binding site will increase the G protein binding site active conformation stability and occupancy on agonist binding. Therefore, it will enhance the allosteric coupling (α), the recruitment of G protein by the receptor and the intracellular receptor activity stimulated by the agonist (Fig. 1e). Additional regulatory effects can be engineered by manipulating stability (K_R) and allosteric coupling simultaneously (Supplementary Fig. 1g–k). (3) Altering the ligand binding affinity (K_A, where $K_A = [AR]/[A][R]$) will affect the ligand concentration triggering receptor activation (that is, ligand potency, half-maximal effective concentration (EC_{50}) or inhibitory concentration (IC_{50}), Supplementary Fig. 1)[27]. In our study, we reprogrammed constitutive and ligand-induced receptor activities through the first two above-mentioned mechanisms. As described below, these functional properties can be rationally engineered through the design of two specific classes (that is, stability and allosteric) of microswitches.

So far, roughly 5% of GPCRs have been structurally characterized, thus limiting the application of rational structure-based protein design. Therefore, we developed a general structure prediction and design method, which is in principle applicable to GPCRs and other membrane receptor classes (Supplementary Fig. 2). First, ligand-free and ligand-bound inactive and active GPCR conformations were modeled by homology to existing structures using the software packages RosettaMembrane and IPHoLD[27,28] (Supplementary Fig. 2, left). Then, we mutated in silico multiple TM positions to all possible 20 amino-acids, and selected microswitches that shift the stability or the structural coupling of specific receptor conformations (Supplementary Fig. 2, right). For example, receptors with increased constitutive activity can be engineered through stability microswitches making more stabilizing contacts in the active versus the inactive ligand-free conformations. On the other hand, receptors with enhanced signaling response to the agonist can be engineered through allosteric microswitches increasing the structural coupling of the ligand-bound site to the active G protein site conformation while decreasing that to the inactive G protein site conformation.

The contribution to the receptor stability of a microswitch is calculated by the scoring function RosettaMembrane and depends on the number and strength of short-distance hydrophobic and polar atomic contacts with neighboring residues[29,30]. Since allosteric protein responses are most sensitive to mutations of coupled residues[10], we approximate the structural coupling by the interactions between the highly coupled allosteric microswitches. Depending on the microswitches' locations, structural couplings involve local or long-range interactions (Methods). Local interactions are calculated through short-range atomic contacts scored by RosettaMembrane[30]. Long-range interactions are calculated by the correlated movements of coupled allosteric microswitches. Long-range structural coupling between microswitches is stronger when the correlation in their motions is higher. Perturbations in correlated movements are rapidly calculated by normal mode analysis (NMA)[31]. NMA is an efficient simulation technique that can capture important functional motions in proteins and has been extensively applied to study the sequence, structure and dynamic origins of protein allostery[31,32] (Methods). The combination of techniques implemented in our approach enables the efficient scanning of billions of possible combinations of designed microswitches modulating stability and long-range structural coupling, which would be intractable using classical MD simulations.

Below, we first describe the validation of our approach by engineering D2 variants with reprogrammed signaling properties. We then further validate the approach by predicting known mutational effects on the signaling activities of diverse GPCRs.

Design of D2 signaling. D2 is involved in many central neurobiological functions and associated with numerous diseases including Parkinson's, Alzheimer's and schizophrenia. Engineered D2s with reprogrammed signaling properties would provide new molecules to better study downstream signaling and behavioral outcomes for example. We modeled D2 in the inactive and active states from the homolog dopamine D3 receptor (D3) and beta2 adrenergic receptor (B2) structures, respectively (Methods). D2 shares high sequence identity in the TM region (>40%) with these homologs. In other receptors sharing lower TM sequence identity with B2, allosteric residues overlapped with those of B2 (refs. [7,8]) (Methods). This suggests that the positions of allosteric residues can be mapped onto D2 using information derived from MD simulations of B2 (ref. [7]). This mapping is then substantially improved using structural details of the D2 models enabling reliable calculations of receptor conformational stability and structural coupling (Methods). We validated the selected designed D2 variants using in vitro G protein Gi activation, fluorescence measurements and intracellular signaling assays[33] (Methods).

Distinct effect of a stability or allosteric microswitch. Since allosteric protein properties are most sensitive to changes in coupled residues, we first tested the accuracy of our approach by mutating single allosteric residues in TM regions distant from the ligand and G protein binding sites. For example, our calculations indicated that three microswitches with distinct effects on stability or structural coupling could be designed at the residue Thr 5.54 (Ballesteros–Weinstein notation[34], which corresponds to D2 position 205). Ile 5.54 was designed as a selective stability microswitch, making more optimal contacts in the active than in the inactive conformation as compared to the native Thr without affecting the structural coupling with other allosteric residues (Fig. 2a–c and Supplementary Table 1). Consequently, it should selectively stabilize the active state even in the absence of ligand. Consistent with the predictions, we observed an increased constitutive activity with a maximal agonist-induced activity similar to wild-type (WT) (Fig. 2a). Conversely, Met 5.54 and Val 5.54 were designed as selective allosteric microswitches inducing no effects on the relative stability of the receptor conformations (that is, similar local contacts in both inactive and active states) but perturbing the structural couplings (Fig. 2d–i and Supplementary Table 1). Met 5.54 selectively increased the structural coupling between the agonist and the G protein binding site in the active state and should therefore enhance the intracellular response to ligand agonists (that is, increase the allosteric coupling α) (Fig. 2f). Conversely, Val 5.54 selectively increased the structural coupling between the agonist and the G protein binding site in the inactive state and should decrease the intracellular response

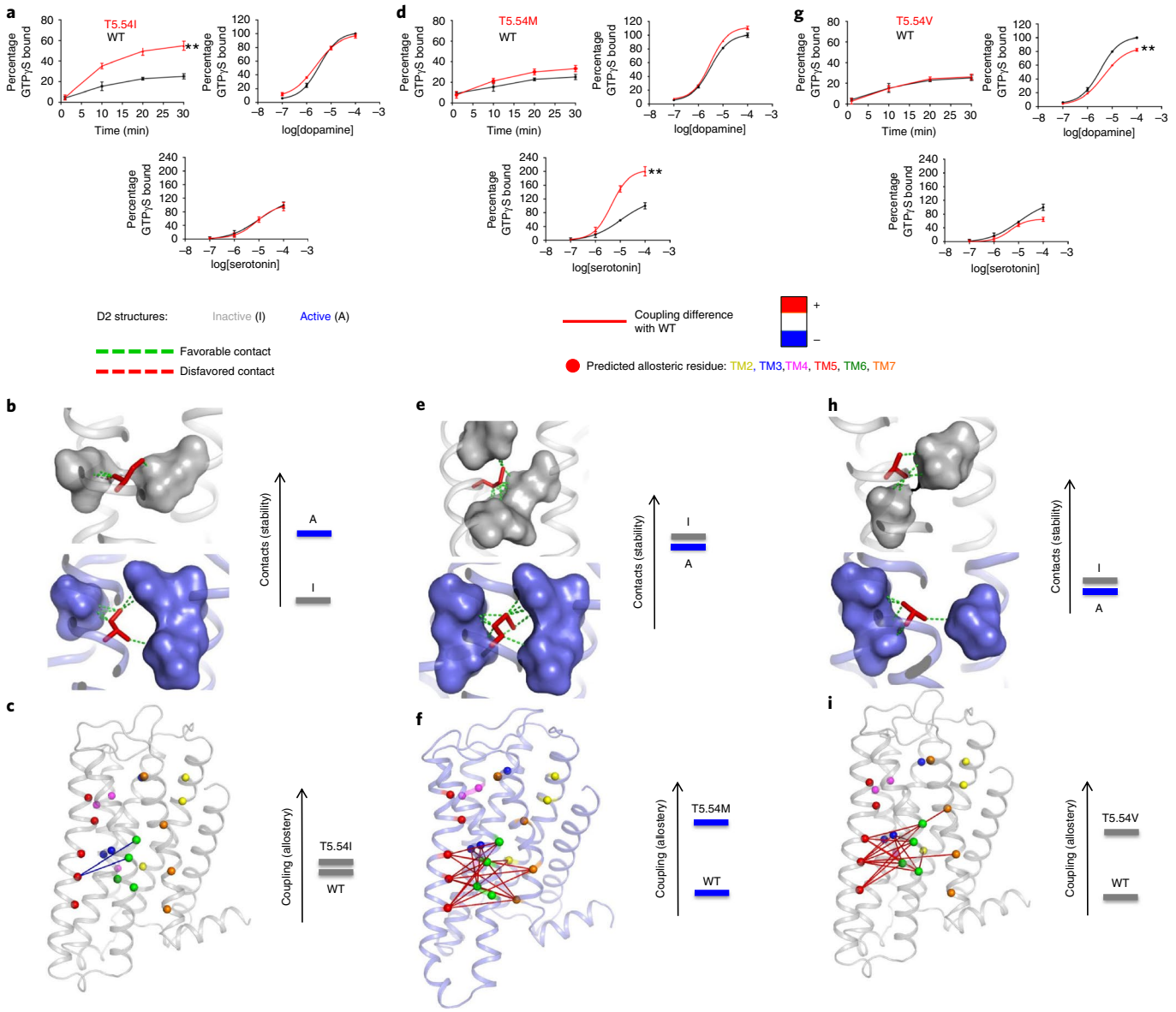

Fig. 2 | Design of single microswitches modulating stability or long-range structural coupling. a–i, Three microswitches at position 205 (5.54), T5.54I (**a**,**b**,**g**), T5.54M (**c**,**d**,**h**) and T5.54V (**e**,**f**,**i**). **a**,**c**,**e**, In vitro measurements of D2 activation (WT, black and design, red) (data shown are mean ± s.d. $^{**}P < 0.05$; two-sided unpaired *t*-test. See detailed statistics in Supplementary Table 1). Left, constitutive (time course); right and bottom, agonist induced (dose response) as a percentage of maximal dopamine induced D2 WT activity. **b**,**d**,**f**, Comparison between local contacts (stability) of active and inactive D2 conformations. **g**,**h**,**i**, Changes in dynamic coupling from WT (differences in correlated motions of amplitude >0.02 measured by NMA, see Methods) induced by the designed microswitch are highlighted by a colored line (red and blue for coupling increase and decrease, respectively). The selected state (that is, inactive, gray or active, blue) is the most perturbed by the mutation. The allosteric residues are indicated as spheres on the structure, colored based on their TM location.

to ligand agonists (that is, decrease the allosteric coupling α) (Fig. 2i and Supplementary Fig. 1a,f). As predicted, both microswitches had no measurable effects on the receptor constitutive activity. Met 5.54 increased receptor activity in vitro by up to 100% in response to the weak agonist serotonin while Val 5.54 substantially decreased receptor activity in response to both dopamine and serotonin (Fig. 2d,g). To achieve these opposite effects, Met 5.54 and Val 5.54 perturbed distinct subnetworks of allosteric residues, consistent with alternative allosteric pathways coupling the extracellular and intracellular sites in the inactive and active receptor conformations[7] (Supplementary Fig. 3).

These results suggested that our approach is sensitive enough to predict the effects of mutations on distinct receptor signaling properties, setting the stage for more extensive protein engineering efforts. Unlike site-directed and deep mutagenesis approaches that often probe only one substitution at a time[22], structure-based computational design can scan through an astronomical number of combinations of mutations to create large changes in sequence, structure and function. We assessed whether D2 variants with a wide diversity of signaling properties could be designed through new networks of microswitches.

Designed D2 receptors stabilized in the active state. Engineering D2 stabilized in an activated form would accelerate the structural characterization of intrinsically unstable active states that often requires formation of a ternary complex between the receptor,

ligand agonist and downstream effectors[35–38]. Highly constitutively activated receptors would also foster the study of the allosteric properties underlying inverse agonism and the discovery of potent long sought-after receptor inhibitors (inverse agonists).

To achieve high conformational stability, we designed stability microswitches in four regions (R1, R2, R3 and R4) spanning the entire TM domain (Fig. 3a). As assessed by functional assays, fluorescence spectroscopy and structure modeling, each designed region partially activates the receptor by adopting specific local active conformations in absence of ligands or Gi (Fig. 3 and Supplementary Table 2). Fluorescence spectra were recorded for a fluorophore monobromobimane coupled to the intracellular end of TMH6 that undergoes the largest conformational changes on receptor activation[36] (Fig. 3b). As observed for the B2, by shifting the receptor to the active state conformation, binding of agonist, Gi or both leads to quenching of monobromobimane coupled to WT D2 (ref. [39]) (Fig. 3c). The level of spectral change corroborates the extent of active state stabilization and receptor activation induced by ligand or G protein binding (Fig. 3c, right). Therefore, if designed microswitches partially mimic the ligand effects on receptor structure and activity, then ligand binding to the designed receptor should result in reduced spectral changes compared to WT (Methods).

On the extracellular side of TMH6 and TMH7 forming part of the ligand binding site (region R1), we designed three microswitches shifting R1 toward the active conformation without substantially perturbing long-range structural couplings (Fig. 3d and Supplementary Table 3). Consequently, the conformational changes were efficiently propagated over a long-distance, stabilizing the intracellular active conformation and increasing the receptor constitutive activity without preventing the downregulation by the inverse agonist spiperone. Smaller fluorescent changes on agonist binding compared to WT suggest that the designed microswitches partially mimic the agonist-induced conformational shifts corroborating our structural models (Supplementary Fig. 4). Deeply buried in the lipid membrane, the R2 region connects the extracellular and intracellular sides of TMH5 and TMH6, but R2 only partially overlaps with the highly conserved 'transmission' region in rhodopsin-like GPCRs[16] (Fig. 3e). Carefully designed microswitches shifted the region toward the active conformation without substantially perturbing the long-range structural couplings, despite multiple mutations at allosteric residues (positions 5.51 and 5.54). Consistent with the predictions, the R2 variant displayed increased constitutive activity from WT but was fully switched off on spiperone binding. Agonist and Gi binding to the R2 variant displayed a unique combination of fluorescent spectral shifts, consistent with specific residue movements designed at the TMH5–TMH6 helical interface as predicted by our structural models (Supplementary Fig. 4). The R3 region undergoes the largest conformational changes on receptor activation and also comprises the highest number of allosteric residues among the designed regions (Fig. 3f). The microswitches we engineered in the R3 region induced the largest conformational stability and structural coupling changes of all variants (Supplementary Tables 2 and 3). Fluorescence spectroscopy, modeling and Gi activation measurements confirmed that the region is locked in an active conformation that partially activates the receptor and does not respond to inverse agonist binding (Fig. 3f and Supplementary Fig. 4). R4 is the region closest to the Gi intracellular binding site and incorporates the highly conserved NPxxY motif. We designed microswitches to rewire the interaction networks between TMH2 and TMH7, shifting the local R4 region toward the active conformation (Fig. 3g). One of the microswitches at the conserved allosteric residue Y7.53 also decreased the structural coupling in the inactive state, leading to a loss in inverse agonist potency. As revealed by the reduced spectral changes on Gi binding and our modeling, the microswitches stabilize R4 in a conformation partially mimicking the Gi-bound WT receptor (Fig. 3g and Supplementary Fig. 4).

We then analyzed the structural coupling properties of the designed R1–4 variants using NMA to understand the origin of their distinct responses to spiperone. We observed a strong correlation between the loss in ligand potency/efficacy and the fraction of allosteric networks affected by the designed microswitches (Supplementary Fig. 5).

Allosteric microswitches reprogram D2 ligand sensing. Following our successful allosteric microswitch design at the position 5.54 (Fig. 2), we designed other predicted allosteric residues with the goal of reprogramming D2 into a biosensor with altered signaling responses to diverse ligands (Fig. 4a). We focused on sites most distant from both ligand and G protein binding sites to primarily induce long-range allosteric effects. We scanned all possible amino-acid substitutions and selected those that were predicted to least affect constitutive activity. We selected a representative subset of 15 designed point mutations for experimental validation that covered all TMHs bearing allosteric sites (with the exception of TMH4 and TMH7), and were predicted to differently modulate ligand responses (Supplementary Table 4). Signaling responses were measured for the native potent agonist dopamine and the nonnative serotonin that activates D2 WT only very weakly. Except for two mutations, the experimentally observed effects were correctly predicted using our calculations of long-range structural coupling (Methods, Supplementary Table 4 and Supplementary Fig. 6). Similar to T5.54M, we identified three sites on TMH6 (6.41, 6.44, 6.47) that significantly enhanced the potency of dopamine (Fig. 4b). These gain of function mutations increased also the signaling responses to serotonin, which reached the same efficacy with D2 F6.44I as with 5HT1AR WT, a GPCR naturally evolved to sense and respond to serotonin (Fig. 4b). Despite the high sensitivity of D2 F6.44I for serotonin, the ligand potency for that D2 variant remained well below that for 5HT1AR WT, indicating that ligand efficacy and potency can be optimized differently. Our calculations predicted also neutral mutations that did not modify the potency of dopamine (Fig. 4c). Last, in addition to T5.54V (Fig. 2), we identified three sites on TMH3, 5 and 6 that significantly decreased the potency and efficacy of dopamine (Fig. 4d). Mutations I3.40T and I3.40L substantially increased the structural coupling of the agonist to the inactive G protein binding site, consistent with reduced responses to dopamine (Supplementary Fig. 6). Our calculations suggest that the native amino-acid isoleucine at position 3.40, which is highly conserved among class A GPCRs, is optimal for coupling ligand agonists to Gi. Overall, we observed that all the designed D2 with enhanced sensitivity to dopamine had also higher sensitivity to serotonin, suggesting that both ligands share similar allosteric pathways to couple to Gi.

Designed microswitches define multiple allosteric paths. To design biosensors with very high sensitivity to ligands, we combined all gain of function mutations and created double mutant D2 variants. We observed a wide spectrum of effects ranging from a nearly complete loss of signaling responses to additive effects on ligand potency and efficacy (Fig. 4e). For almost all double mutants, our structural coupling calculations predicted correctly the classes of effects (that is, gain, neutral and loss of function) (Supplementary Table 4), which strongly depend on the relative location of the designed microswitches. Loss of function coincided with very close proximity between the allosteric mutations, which were structurally incompatible. Nonantagonizing mutations that were only three residues apart displayed no additivity and, at best, behaved similarly to the highest gain of function single point mutant (Fig. 4f,g). Variants incorporating the most distant pairs of mutations (5.54/6.47, 6.41/6.47) displayed significant additivity in serotonin potency and efficacy (Fig. 4h,i), including the T5.54M-C6.47L variant that responded to serotonin very similarly to the native

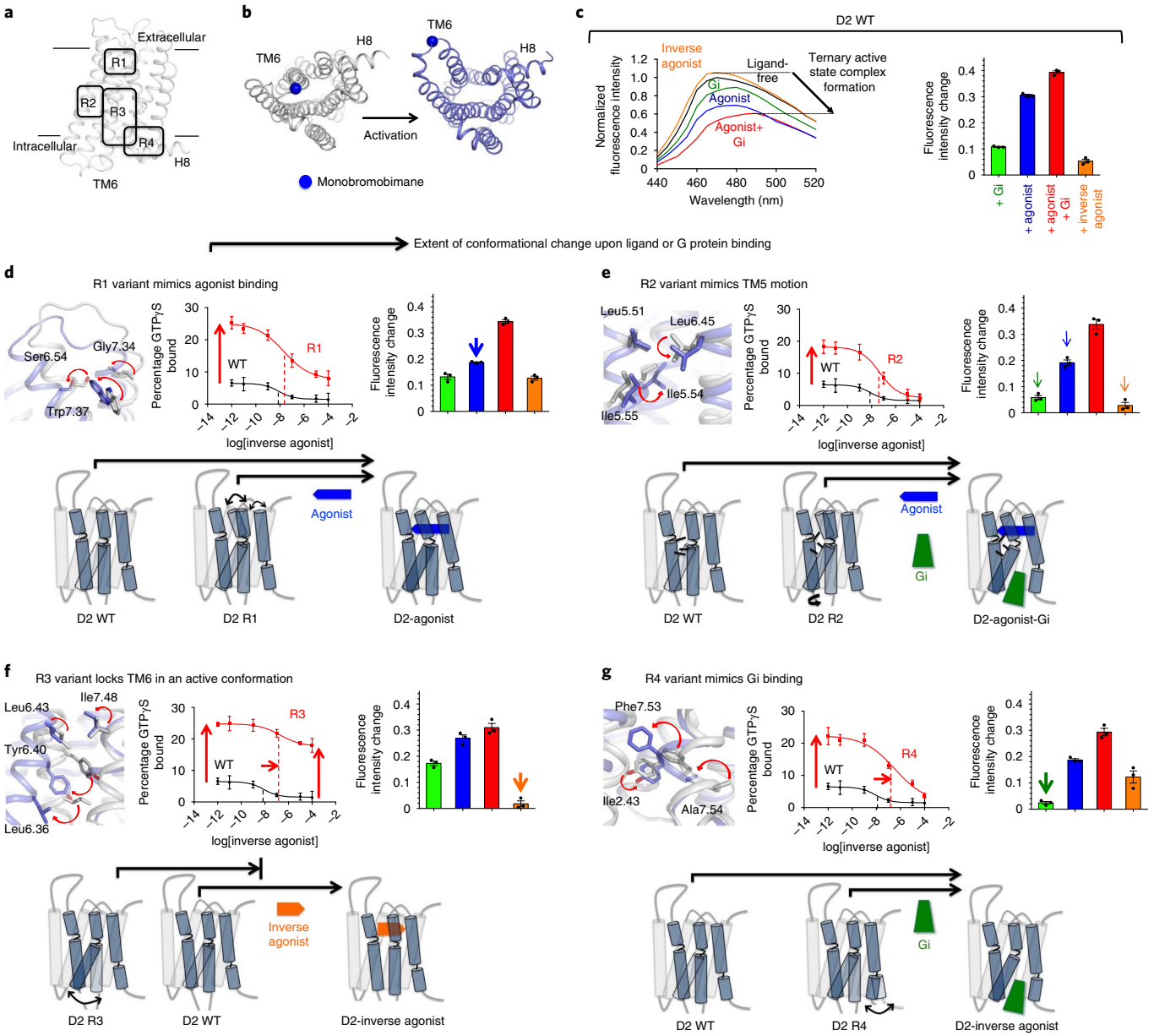

Fig. 3 | Designed microswitches stabilize distinct local active state structures. a, R1–R4 designed regions span the entire TM domain. **b**, The cytoplasmic end of TMH6 is coupled to a fluorophore whose fluorescence is quenched and red-shifted on receptor activation. **c**, Left, the largest shifts are reached when D2 is bound to both agonist and Gi in a ternary active state complex. One representative experiment is shown. Right, changes in maximal fluorescence intensity on binding to ligand or Gi are normalized to that induced by binding of both agonist and Gi. The absolute values of the changes from $N=3$ independent experiments are reported. **d**–**g**, Changes in receptor activity, fluorescence and proposed local conformational changes are indicated for microswitches designed in regions R1 (**d**), R2 (**e**), R3 (**f**) and R4 (**g**). The designed microswitches are indicated in sticks on the inactive (gray) and active (blue) state D2 structures. In vitro measured downregulation of receptor activity by spiperone are reported for D2 WT (black) and designed variants (red). Receptor activity is reported as a percentage of maximal dopamine induced D2 WT activity (see detailed statistics in Supplementary Table 3). The largest changes from WT are indicated by a red arrow in the activity plots. EC_{50}s are indicated by a dotted line. The largest fluorescence intensity changes compared to D2 WT or to other local designed region variants are indicated by a colored arrow in the histograms (fluorescence data shown are mean ± s.e.m. from $N=3$ independent experiments). The structural interpretation of the modeling results (Supplementary Fig. 4) is highlighted using a schematic cartoon representation of the D2 structure where TMHs 5, 6 and 7 are shaded in dark gray. When one of these helices occupies both an inactive and active conformation, darker gray indicates higher occupancy. The length of the black straight arrow indicates the extent of the conformational change induced by ligand or Gi binding. Black curved arrows indicate local structural changes induced by the designed microswitches. Black lines in R2 on TMHs 5 and 6 indicate designed microswitches.

serotonin 5HT1AR receptor. C6.47 is a key connector between TMH6 and TMH7 while T5.54, L6.41 and F6.44 mainly connect TMH5 with TMH6, indicating that individual designed microswitches can modulate the structural coupling between the extracellular and intracellular sites through either the TMH5-6 or the TMH6-7 interfaces. Additive effects occur when distant mutations enhance structural coupling of distinct TMH interfaces and strongly suggest the existence of two allosteric subpathways involving TMH5-6 and TMH6-7 dynamically coupled interactions that can be independently optimized (Supplementary Fig. 7).

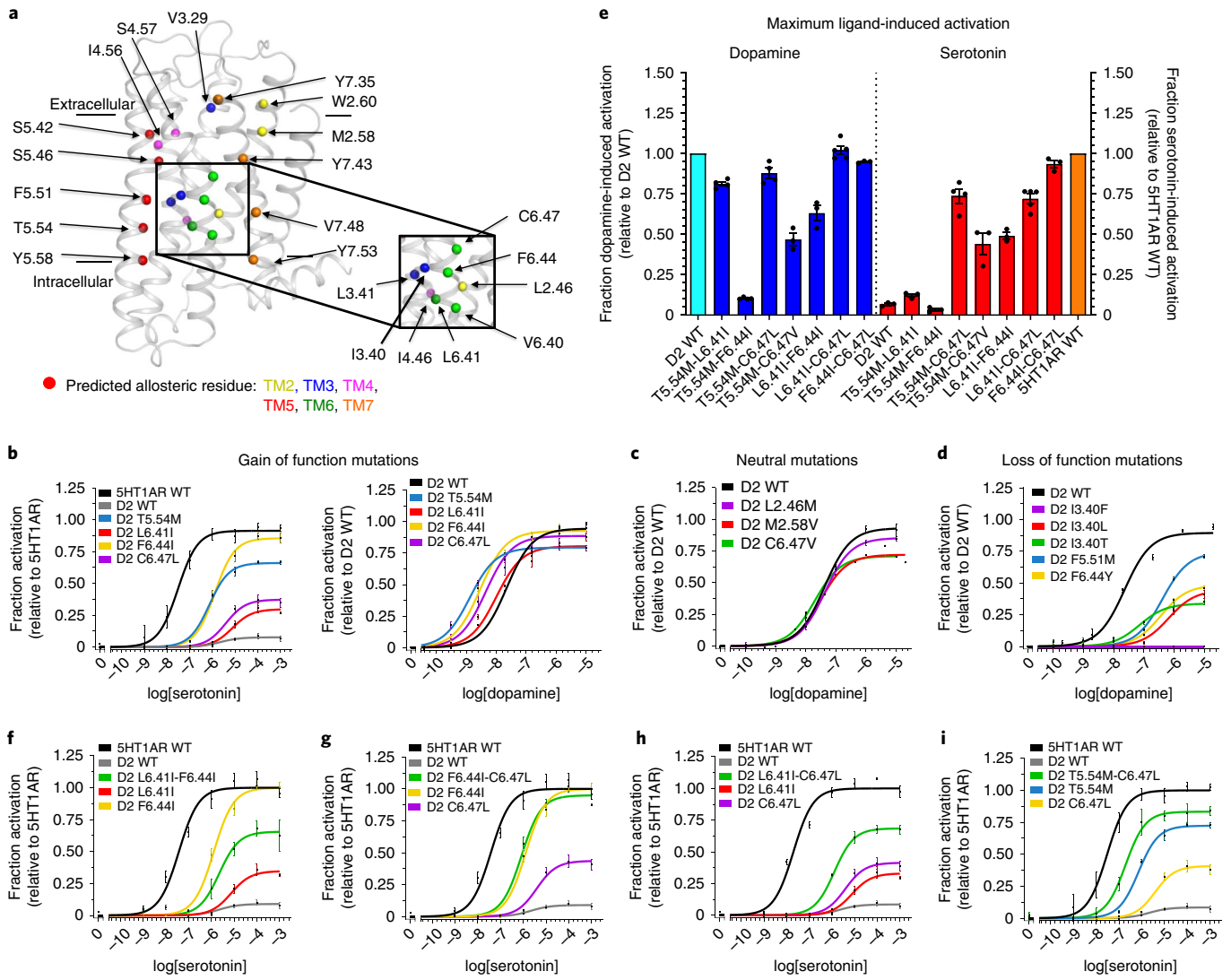

Fig. 4 | Designed allosteric microswitches reprogram ligand sensing and signaling responses. a, Allosteric sites predicted by MD simulations are indicated as spheres on the D2 model structure, and colored based on their TM location. **b**–**i**, D2 activation on agonist dopamine or serotonin binding measured using the cell-based FLIPR assay. Agonist induced (dose response) as a percentage of maximal dopamine induced D2 WT activity or serotonin induced 5HT1R WT activity. Reported dose response curves (**b**–**d**, **f**–**i**) are from $N=3$ representative independent experiments and data shown are mean ± s.e.m. **b**–**d**, Designed point mutations are classified based on their signaling effects: gain of function (**b**), neutral (**c**) and loss of function (**d**). **e**–**i**, Double mutants incorporating gain of function mutations. **e**, Dopamine and serotonin induced responses of double mutants incorporating gain of function mutations (see detailed statistics in Supplementary Table 4). **f**,**g**, Serotonin induced responses by pairs of gain of function mutations that are close in the structure. **h**,**i**, Serotonin induced responses by pairs of gain of function mutations that are distant in the structure. Agonist induced (dose response) as a percentage of maximal serotonin induced 5HT1R WT activity. Serotonin induced D2 WT activity is also represented for comparison.

New model of GPCR regulation and evolution. Overall, our results provide new fundamental insights into the molecular mechanism of GPCR allosteric signaling and evolution. So far, the classical pre-eminent model of class A GPCR signaling primarily involved a few highly conserved allosteric microswitches (that is, DRY ionic lock on TMH3, PIF transmission switch on TMH5,6, W toggle switch on TMH6 and NPxxY motif on TMH7, Fig. 5a) that trigger consensus structural changes in the receptor during activation[16–18] (Fig. 5b). Mutation to alanine of most of these sites led to severe loss in ligand-induced receptor signaling, indicating that the native switches are close-to-optimal for signal transduction (Fig. 5c)[40]. However, these motifs are not in direct contact and their connections throughout the receptor structure that define the allosteric signal transduction pathways have remained elusive. Most importantly, a molecular mechanism of signal transduction involving only a few highly conserved and close-to-optimal signaling switches does not explain the large spectrum of signaling responses displayed by GPCRs.

Here, we deconstructed the determinants of signal transduction and uncovered two new classes of microswitches that modulate specific receptor signaling properties. Unlike the above-mentioned consensus microswitches, they exhibit a large diversity in sequence conservation and structural movements and could not be easily detected (Fig. 5d,e,g). The class of 'stability' microswitches that we now call 'conformational selectors' were identified in regions undergoing the largest movements on receptor activation (Fig. 5e). By forming distinct contacts in different conformations, they selectively control the time spent by the receptor in each state. Engineering these sites reprograms selectively the receptor conformational stability and constitutive activity (Fig. 5f). The class of 'allosteric' microswitches that we now call 'allosteric propagators'

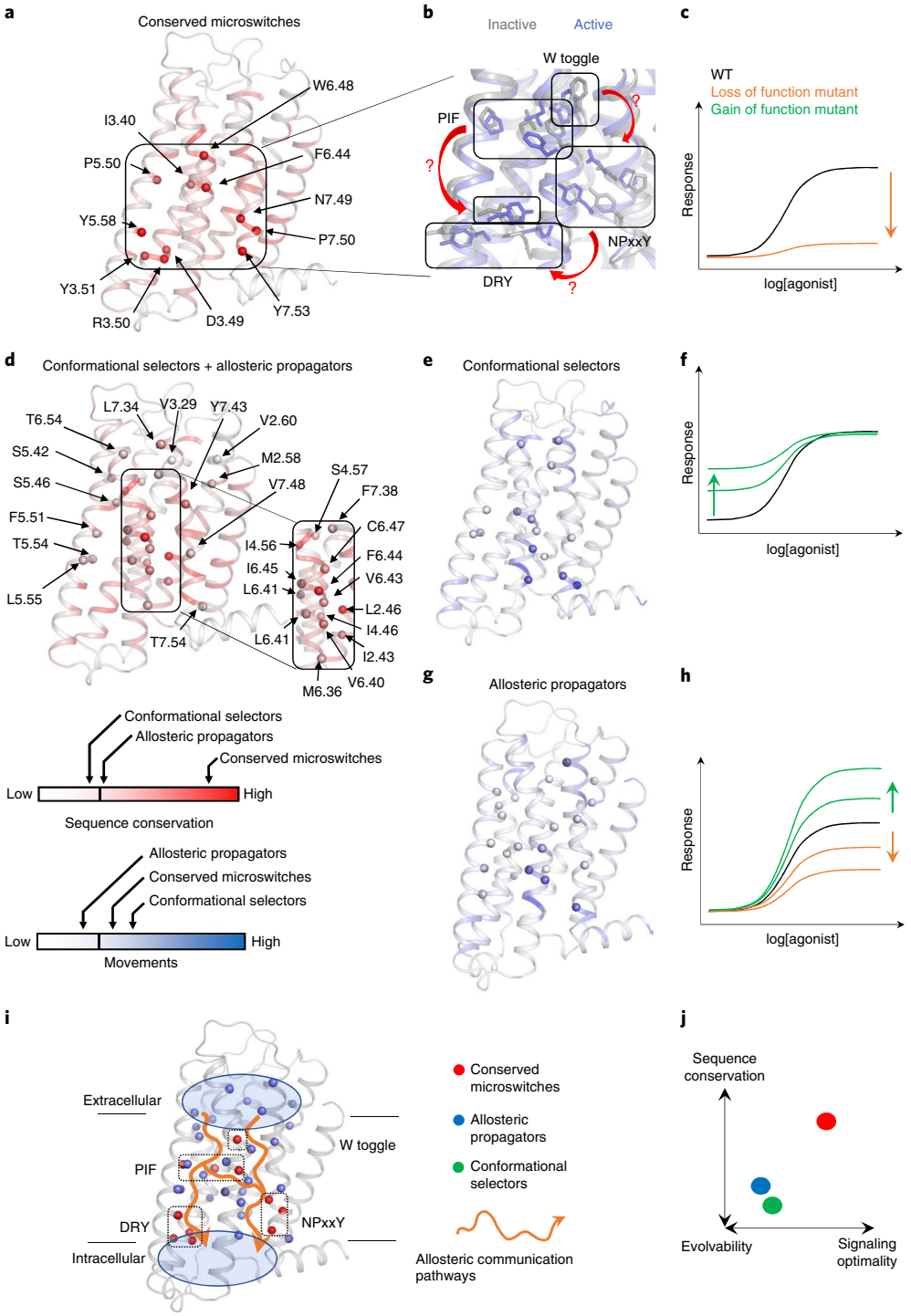

Fig. 5 | A high-resolution mechanism for the regulation and evolution of GPCR allosteric signaling properties. a–c, Properties of conserved allosteric microswitches. **a**, Conserved allosteric microswitches shown in spheres colored by sequence conservation (high, red; low, white). **b**, Conformational changes of the conserved allosteric microswitches represented in sticks on receptor activation. Red arrows with question marks represent the unknown connectivity linking the conserved microswitches. **c**, Schematic agonist-induced signal response curve representing the deleterious effects of alanine mutations of most conserved microswitches. **d–h**, Properties of conformational selectors and allosteric propagators. **d**, Conformational selectors and allosteric propagators shown in spheres colored by sequence conservation (high, red; low, white). The scale below recapitulates the average sequence conservation for each class of residues in class A GPCRs (the back bar represents the average over all residues). **e**, Conformational changes of the conformational selectors represented as spheres on receptor activation (blue, high; white, low). **f**, Schematic agonist-induced signal response curve representing the effects of conformational selector mutations stabilizing the receptor active state. **g**, Conformational changes of the allosteric propagators represented as spheres on receptor activation (blue, high; white, low). The scale below recapitulates the average movement for each class of residues (the back bar represents the average over all residues). **h**, Schematic agonist-induced signal response curve representing the effects of allosteric propagator mutations modulating the coupling between agonist and downstream effectors. **i**, High-resolution schematic mapping of GPCR allosteric signal transductions where allosteric propagators connect the conserved microswitches and define several quasi-independent allosteric subpathways. **j**, Schematic diagram representing the relationship between sequence conservation, signaling optimality and evolvability of each class of allosteric residues.

usually do not display major structural changes between states (Fig. 5g) but are dynamically coupled and can propagate signals over long-distances. As such, they represent key regulators of allosteric signaling function. Engineering these sites can modulate selectively the responses to ligands by enhancing or decreasing the receptor allosteric sensing properties (Fig. 5h).

From this expanded molecular description emerges a model of evolution of allosteric regulation where sparse conserved allosteric sites are connected through a network of allosteric propagators that control their coupling and can modulate the strength and direction of the allosteric communication pathways (Fig. 5i). Conserved microswitches are often close-to-optimal for signal transduction as most amino-acid substitutions at these sites are deleterious. Consistent with a high level of sequence conservation, they correspond to highly constrained sites with low potential for evolvability and signaling diversity (Fig. 5j). By contrast, 'allosteric propagators' appear farther away from signaling optimality as several designed mutants enhanced signaling functions. Consistent with a lower level of sequence conservation, they provide key sites for evolution of a wide range of allosteric signaling responses in class A GPCRs by modulating the coupling and pathways between the conserved microswitches. Evolutionary coupling between residues in GPCRs were found to maintain ligand responses to those of native receptors[11]. By contrast, our findings indicate that physical coupling can drive the evolution of a wide range of receptor signaling properties for generating functional diversity.

Prediction accuracy and limitations of the method. To assess the broad use of the computational approach, we calculated its prediction accuracy. Because the designed receptors were selected for experimental validation based on calculated criteria only (Methods), they represent true blind predictions and a stringent dataset for validating our approach. We performed qualitative and quantitative comparisons between calculated and measured properties (Methods). Qualitatively, the direction of the changes in constitutive and ligand-induced activities from WT were correctly predicted for 81 and 82% of the designs, respectively (Supplementary Fig. 8, see Methods). Changes in ligand-free receptor energies and calculated long-range allosteric couplings quantitatively correlated fairly well with changes in constitutive activities (Pearson correlation coefficient $r=0.68$) and in ligand potency ($r=0.54$), respectively (Supplementary Fig. 9, see Methods). To expand the validation of the approach, we predicted the signaling effects of 109 known mutations on several GPCRs. The prediction accuracy on these additional datasets (r varying between 0.55 and 0.69) was comparable to that observed with our designs (Supplementary Figs. 10 and 11, see Methods). These results indicate that the computational approach has strong qualitative and fair quantitative predictive power, similar to structure-based predictions of mutational effects on protein stability by Rosetta[41].

Nevertheless, the predictions are not yet quantitatively very accurate, which currently precludes a complete mechanistic understanding of every design's success or failures. Since the approach relies on the ability to predict the effects of mutations on protein structures, which remains challenging when modeling protein conformations by homology to existing structures, structure prediction inaccuracies are likely a main factor behind the lack of precise quantitative predictions.

Despite its approximation, the two-state model seems to be sufficient to reprogram the receptor constitutive activity and the activity induced by a particular ligand. However, GPCRs can adopt multiple conformational states and more complex design scenarios involving multiple extracellular ligands, allosteric modulators and/or distinct intracellular signaling partners would necessitate a multi-state approach. In addition to accurate structure predictions, the success of our approach relies also on the ability to design residue–residue interactions that are distinct in different states to achieve selective functional effects. Therefore, if no structural information from close homologs is available on these states and/or if their conformations are too similar, the current implementation may not be accurate enough for such complex multi-state design scenarios.

Discussion

We developed a method for designing allosteric functions in membrane receptors. The method first predicts allosteric sites and pathways in receptor structures using MD simulations. It then combines multi-state design and normal mode calculations to de novo design residue microswitches modulating receptor conformational stability or long-range coupling between allosteric sites that reprogram specific allosteric signaling properties.

Using this approach, we designed dopamine D2 receptors displaying an unprecedented spectrum of signaling activities with a success rate higher than 80% (Supplementary Fig. 8, see Methods). We were able to repurpose the D2 receptor to trigger potent signaling responses on sensing the noncognate ligand serotonin, which constitute, to our knowledge, the first GPCR-based biosensor engineered by computational structure-based protein design. We also reliably predicted the effects of more than 100 mutations on the signaling activity of diverse rhodopsin class GPCRs (Supplementary Figs. 9 and 10, see Methods), which represents the largest benchmark of its kind. Our method requires only the structures of homolog proteins, and does not rely on evolutionary or functional information[11,42,43]. Therefore, any protein with available structural homologs may be targeted and, in principle, de novo design of allosteric proteins can be envisioned with the technique. Overall, the computational approach provides an effective mean to design receptor stability and function that largely outperforms random mutagenesis approaches in efficiency and success rate.

Our study reveals fundamental new insights into the mechanisms of regulation and evolution of GPCR signaling with the existence of two unforeseen 'conformational selectors' and 'allosteric propagators' classes of microswitches that perform largely distinct signaling functions (Fig. 5). Unlike the highly conserved allosteric microswitches that have been the focus of most studies so far, these microswitches have higher potential for evolvability and provide the backbone for coding signaling diversity such as the modulation of constitutive activity, ligand efficacy and potency as demonstrated in our study and likely signaling bias as well. Our results also uncovered the existence of topologically distinct allosteric subpathways that function quasi-independently in the TM core of the D2 receptor. Their coupling can be modulated separately and they can act synergistically to achieve optimal intracellular effector activation. This particular allosteric network design offers a number of advantages for coding large spectrum of signaling response strengths, fine-grained tuning responses to ligands potentiating distinct signal transduction routes, while providing inherent robustness during evolution. In conclusion, while allosteric pathways in the transmembrane and intracellular regions were largely viewed as conserved routes preserving consensus long-range communications and signaling functions in GPCRs, our study reveals that they actually constitute a critical backbone for driving the evolution of signaling and functional diversity, which redefines our understanding of GPCR allostery.

Overall, our strategy should prove particularly useful for designing new regulatory pathways and repurposing membrane receptors as biosensors to a vast array of chemical molecules. Foreseeable applications of our method include the de novo design of allosteric biosensors and signaling receptors to reprogram cellular functions that is at the heart of current engineering approaches for synthetic biology and cancer immunotherapeutic applications.

Online content

Any methods, additional references, Nature Research reporting summaries, source data, extended data, supplementary information,

acknowledgements, peer review information; details of author contributions and competing interests; and statements of data and code availability are available at https://doi.org/10.1038/s41589-019-0407-2.

Received: 18 September 2018; Accepted: 10 October 2019;
Published online: 02 December 2019

References

1. Suel, G. M., Lockless, S. W., Wall, M. A. & Ranganathan, R. Evolutionarily conserved networks of residues mediate allosteric communication in proteins. *Nat. Struct. Biol.* **10**, 59–69 (2003).
2. Reynolds, K. A., McLaughlin, R. N. & Ranganathan, R. Hot spots for allosteric regulation on protein surfaces. *Cell* **147**, 1564–1575 (2011).
3. Monod, J., Wyman, J. & Changeux, J. P. On the nature of allosteric transitions: a plausible model. *J. Mol. Biol.* **12**, 88–118 (1965).
4. Cui, Q. & Karplus, M. Allostery and cooperativity revisited. *Protein Sci.* **17**, 1295–1307 (2008).
5. Luque, I., Leavitt, S. A. & Freire, E. The linkage between protein folding and functional cooperativity: two sides of the same coin? *Annu Rev. Biophys. Biomol. Struct.* **31**, 235–256 (2002).
6. Clarkson, M. W., Gilmore, S. A., Edgell, M. H. & Lee, A. L. Dynamic coupling and allosteric behavior in a nonallosteric protein. *Biochemistry* **45**, 7693–7699 (2006).
7. Bhattacharya, S. & Vaidehi, N. Differences in allosteric communication pipelines in the inactive and active states of a GPCR. *Biophys. J.* **107**, 422–434 (2014).
8. Miao, Y., Nichols, S. E., Gasper, P. M., Metzger, V. T. & McCammon, J. A. Activation and dynamic network of the M2 muscarinic receptor. *Proc. Natl Acad. Sci. USA* **110**, 10982–10987 (2013).
9. Kohlhoff, K. J. et al. Cloud-based simulations on google exacycle reveal ligand modulation of GPCR activation pathways. *Nat. Chem.* **6**, 15–21 (2014).
10. McLaughlin, R. N. Jr., Poelwijk, F. J., Raman, A., Gosal, W. S. & Ranganathan, R. The spatial architecture of protein function and adaptation. *Nature* **491**, 138–142 (2012).
11. Sung, Y. M., Wilkins, A. D., Rodriguez, G. J., Wensel, T. G. & Lichtarge, O. Intramolecular allosteric communication in dopamine D2 receptor revealed by evolutionary amino acid covariation. *Proc. Natl Acad. Sci. USA* **113**, 3539–3544 (2016).
12. Rosenbaum, D. M., Rasmussen, S. G. & Kobilka, B. K. The structure and function of G-protein-coupled receptors. *Nature* **459**, 356–363 (2009).
13. Tsai, C. J. & Nussinov, R. A unified view of 'how allostery works'. *PLoS Comput. Biol.* **10**, e1003394 (2014).
14. Motlagh, H. N., Wrabl, J. O., Li, J. & Hilser, V. J. The ensemble nature of allostery. *Nature* **508**, 331–339 (2014).
15. Wisler, J. W., Xiao, K., Thomsen, A. R. & Lefkowitz, R. J. Recent developments in biased agonism. *Curr. Opin. Cell Biol.* **27**, 18–24 (2014).
16. Venkatakrishnan, A. J. et al. Molecular signatures of G-protein-coupled receptors. *Nature* **494**, 185–194 (2013).
17. Dror, R. O. et al. Activation mechanism of the beta2-adrenergic receptor. *Proc. Natl Acad. Sci. USA* **108**, 18684–18689 (2011).
18. Ahuja, S. & Smith, S. O. Multiple switches in G protein-coupled receptor activation. *Trends Pharm. Sci.* **30**, 494–502 (2009).
19. Katritch, V., Cherezov, V. & Stevens, R. C. Diversity and modularity of G protein-coupled receptor structures. *Trends Pharm. Sci.* **33**, 17–27 (2012).
20. Flock, T. et al. Selectivity determinants of GPCR-G-protein binding. *Nature* **545**, 317–322 (2017).
21. Scott, D. J., Kummer, L., Tremmel, D. & Pluckthun, A. Stabilizing membrane proteins through protein engineering. *Curr. Opin. Chem. Biol.* **17**, 427–435 (2013).
22. Magnani, F., Shibata, Y., Serrano-Vega, M. J. & Tate, C. G. Co-evolving stability and conformational homogeneity of the human adenosine A2a receptor. *Proc. Natl Acad. Sci. USA* **105**, 10744–10749 (2008).
23. Egloff, P. et al. Structure of signaling-competent neurotensin receptor 1 obtained by directed evolution in *Escherichia coli*. *Proc. Natl Acad. Sci. USA* **111**, E655–E662 (2014).
24. Sarkar, C. A. et al. Directed evolution of a G protein-coupled receptor for expression, stability, and binding selectivity. *Proc. Natl Acad. Sci. USA* **105**, 14808–14813 (2008).
25. Ye, L., Van Eps, N., Zimmer, M., Ernst, O. P. & Prosser, R. S. Activation of the A2A adenosine G-protein-coupled receptor by conformational selection. *Nature* **533**, 265–268 (2016).
26. LeVine, M. V. & Weinstein, H. AIM for allostery: using the Ising model to understand information processing and transmission in allosteric biomolecular systems. *Entropy* **17**, 2895–2918 (2015).
27. Feng, X., Ambia, J., Chen, K. M., Young, M. & Barth, P. Computational design of ligand-binding membrane receptors with high selectivity. *Nat. Chem. Biol.* **13**, 715–723 (2017).
28. Chen, K. Y., Sun, J., Salvo, J. S., Baker, D. & Barth, P. High-resolution modeling of transmembrane helical protein structures from distant homologues. *PLoS Comput. Biol.* **10**, e1003636 (2014).
29. Barth, P., Schonbrun, J. & Baker, D. Toward high-resolution prediction and design of transmembrane helical protein structures. *Proc. Natl Acad. Sci. USA* **104**, 15682–15687 (2007).
30. Chen, K. Y., Zhou, F., Fryszczyn, B. G. & Barth, P. Naturally evolved G protein-coupled receptors adopt metastable conformations. *Proc. Natl Acad. Sci. USA* **109**, 13284–13289 (2012).
31. Perica, T. et al. Evolution of oligomeric state through allosteric pathways that mimic ligand binding. *Science* **346**, 1254346 (2014).
32. Bahar, I., Lezon, T. R., Yang, L. W. & Eyal, E. Global dynamics of proteins: bridging between structure and function. *Annu. Rev. Biophys.* **39**, 23–42 (2010).
33. J Luo, Y Zhu, M Zhu, H Hu, 2011 Cell-based calcium assay for medium to high throughput screening of TRP channel functions using FlexStation 3. J. Vis. Exp. 17.
34. Ballesteros, J. A. & Weinstein, H. Integrated methods for the construction of three-dimensional models and computational probing of structure-function relations in G protein-coupled receptors. *Methods Neurosci.* **25**, 366–428 (1995).
35. Kang, Y. et al. Crystal structure of rhodopsin bound to arrestin by femtosecond X-ray laser. *Nature* **523**, 561–567 (2015).
36. Rasmussen, S. G. et al. Crystal structure of the beta2 adrenergic receptor-Gs protein complex. *Nature* **477**, 549–555 (2011).
37. Koehl, A. et al. Structure of the micro-opioid receptor-Gi protein complex. *Nature* **558**, 547–552 (2018).
38. Carpenter, B., Nehme, R., Warne, T., Leslie, A. G. & Tate, C. G. Structure of the adenosine A(2A) receptor bound to an engineered G protein. *Nature* **536**, 104–107 (2016).
39. Yao, X. J. et al. The effect of ligand efficacy on the formation and stability of a GPCR-G protein complex. *Proc. Natl Acad. Sci. USA* **106**, 9501–9506 (2009).
40. Isberg, V. et al. GPCRdb: an information system for G protein-coupled receptors. *Nucleic Acids Res.* **45**, 2936 (2017).
41. Kellogg, E. H., Leaver-Fay, A. & Baker, D. Role of conformational sampling in computing mutation-induced changes in protein structure and stability. *Proteins* **79**, 830–838 (2011).
42. Rodriguez, G. J., Yao, R., Lichtarge, O. & Wensel, T. G. Evolution-guided discovery and recoding of allosteric pathway specificity determinants in psychoactive bioamine receptors. *Proc. Natl Acad. Sci. USA* **107**, 7787–7792 (2010).
43. Schonegge, A. M. et al. Evolutionary action and structural basis of the allosteric switch controlling beta2AR functional selectivity. *Nat. Commun.* **8**, 2169 (2017).

Methods

Mutagenesis and expression of receptors. Quickchange PCR mutagenesis was performed on *DRD2* gene (isoform 1 of *DRD2* (http://www.uniprot.org/uniprot/P14416.fasta)) in pcDNA3.1(+) from the complementary DNA library. Sequenced mutant plasmids were transiently transfected using lipofectamine into human embryonic kidney 293T (HEK293T) cells. Briefly, 5×10^6 cells were plated on 10 cm tissue culture plates and grown overnight. This was followed by transfection with lipofectamine 2000 and 15 µg of DNA per plate. After 24 h, transfection medium was replaced with standard growth medium (DMEM supplemented with L-glutamine (2 mM), penicillin (100 mg ml^{-1}), streptomycin (100 mg ml^{-1}) and fetal bovine serum (10%)) and cells were grown for an additional 24 h before collection.

Membrane preparation. Membranes were prepared from transfected cells using sucrose gradient centrifugation as previously described[44]. Briefly, cells from 10 cm plates were collected by cell scraper with PBS solution. Cells were pelleted and resuspended in cold hypotonic buffer (1 mM Tris-HCL, pH 6.8, 10 mM EDTA, protease inhibitor cocktail). Cells were forced through a 26-gauge needle three times. The cell lysate was layered onto a 38% sucrose solution in buffer A (150 mM NaCl, 1 mM MgCl, 10 mM EDTA, 20 mM Tris-HCl, pH 6.8, protease inhibitor cocktail) in SW-28 ultracentrifuge tubes. Cells were centrifuged at 15,000 r.p.m. at 4 °C for 20 min, followed by collection of the interface band with an 18-gauge needle. The collected solution was transferred to Ti-45 ultracentrifuge tubes and the volume brought up to 50 ml with buffer A. The sample was spun at 40,000 r.p.m. at 4 °C for 30 min. The membrane pellets from each 10 cm plate was resuspended in 0.5 ml buffer A and stored at −80 °C in 100 µl aliquots.

D2 purification. D2 variants were partially purified from thawed membrane preparations immediately before assaying via anti-HA agarose beads. Membrane preparations were solubilized with 1% *n*-dodecylmaltoside (DDM) for 1 h at 4 °C, and loaded onto anti-HA agarose beads for 1 h at 4 °C. The beads were washed with tris-buffered saline (TBS) with 0.1% DDM wash buffer three times and hemagglutinin-tagged receptor variants were eluted with hemagglutinin peptide (1 mg ml^{-1} in TBS with 0.1% DDM).

The interpretation of designed mutational effects based on the comparison between receptor activities assumes that the different samples of D2 receptor variants have the same level of purity and contains similar fraction of active receptors. To stringently validate this hypothesis, the levels of purity and activity in all samples of receptor variants after detergent solubilization and purification were measured. Purity of affinity purified D2DR samples was assessed by coomassie-stained SDS–PAGE along with western blots for all receptor variants. All bands observed in the final sample preparations used for the assays were quantified by densitometry. All samples consisted mostly of D2 monomers with very similar levels of purity; that is, ranging from 92 to 95%.

To quantify the fraction of active receptor for each variant, the ability of the receptors to bind the ligand agonist dopamine, which should occur only when the receptor is folded and active, was assessed. Specifically, the maximal amount of bound ligand dopamine per receptor quantity was measured from radioligand binding experiments performed with purified D2 samples and with the same batch of tritium labeled ligand across experiments. The analysis indicated that all purified variants contained a fraction of folded and active receptor that was not significantly different from WT (that is, maximal difference was 8%).

Expression and purification of the G protein Gi. Genes coding Gi2 subunits were cloned into pFastbacI followed by transformation into DH10α cells. Recombinant bacmid DNA was isolated and transfected in Sf9 insect cells with Cellfectin II. The transfected cells were grown at 28 °C for 72 h followed by centrifugation in 15 ml Falcon tubes to pellet cell debris. The supernatant was saved as P1 viral stock. Virus was amplified by infecting Sf9 cells with P1 viral stock solution at a two-fold multiplicity of infection (MOI) and cultured for 72 h before collection. This amplification process was repeated to generate a high-titer P3, which was used for infection and protein expression. P3 stock was used to infect Sf9 cells at an MOI greater than four and gathered 48–60 h post-infection. Cells were washed three times in ice-cold PBS and resuspended in homogenization buffer (10 mM Tris-HCl, 25 mM NaCl, 10 mM $MgCl_2$, 1 mM EGTA, 1 mM DTT, protease inhibitor cocktail, 10 µM GDP, pH 8.0). Gi2 was purified and reconstituted as described previously[45]. Antibodies were purchased from Santa Cruz Biotechnology.

In vitro G protein activation assays. Receptor variants were assayed for their ability to induce guanine nucleotide exchange by the G protein Gi2. To measure constitutive activity the reaction mixture consisted of 4 µM Gi2, 20 µM of [^{35}S]-GTPγS mix, 50 mM Tris-HCl, pH 7.2, 100 mM NaCl, 4 mM $MgCl_2$, 1 mM dithiothreitol. D2 concentrations were ~10 nM per sample as estimated from absorbance at 280 nm of the anti-HA agarose purified samples. For all samples used for reactions, western blots were performed to further assess receptor quantity using monoclonal anti-HA antibody (Thermo Scientific). Reactions were started by adding 150 µl partially purified receptor samples to 300 µl of reaction mixture and incubating on ice over a period of time from 0–30 min for timecourse measurements. To measure ligand-induced D2 activities, increasing amounts of dopamine or spiperone were added to the reaction mixtures. Maximal ligand efficacies were obtained with final ligand concentrations of 20 µM and 1 µM for dopamine and spiperone, respectively. Reactions were stopped by filter binding onto Millipore nitrocellulose filters or Whatman fiberglass filters pretreated with polyethylenimine. Filters were washed three times with ice-cold TBS before incubation with scintillation fluid. Radioactivity counts were measured on a Beckman LS6000 scintillation counter. Mock-transfected samples (using an empty pcDNA vector) and WT receptor were assayed in every experiment as internal controls. Background binding measured by mock-transfected samples was subtracted and activities of receptor variants were normalized relative to WT receptor via densitometry analysis of western blots using ImageJ software. Statistical significance of differences in constitutive or ligand-induced activities was assessed by unpaired two-sided *t*-tests. Nonlinear curve-fitting was performed for each dose response dataset using GraphPad Prism 6. Measurements were taken from distinct samples.

Trp channel activation cell-based assay. HEK293 cells stably expressing TrpC4β channel were kindly provided by M.X. Zhu and were transiently transfected with D2 design variants as described below. FMP2 FLIPR membrane potential assays (Molecular Devices) were performed as previously described[46]. Briefly, the assay uses a fluorescent probe that reacts to cations and is coupled with a nonpermeable quencher. Activation of TrpC4β causes influx of cations leading to the translocation of the fluorescent probe away from the quencher, resulting in increased fluorescence. TrpC4β has been described to be downstream of Gi activation and serves as a reporter for D2 activation. Stable HEK293 cells were cultured in DMEM supplemented with 10% FBS and 1% G418 (selection antibiotic) for use with FLIPR membrane potential assay kits (Molecular Devices). On the day of transfection, cells stably expressing TrpC4β were plated (1.5×10^5 cells per well) onto 96-well clear, flat-bottom plates precoated with poly-D-lysine (Sigma). Cells were transfected with lipofectamine 2000 and the appropriate D2 constructs using optimized DNA quantity for the FLIPR assay (1 ng DNA per well for D2 WT, 0.5 µl lipofectamine per well) and grown for 24 h before assaying. A duplicate plate was transfected and grown for assessment of receptor cell surface expression determined by ELISA using anti-HA antibody as described previously[47]. For each variant, DNA titration experiments were performed to determine the DNA quantity required to match the surface expression of D2 WT. Background signal was removed by subtracting fluorescence signals from mock-transfected cells. Cells were treated with either dopamine or serotonin to measure activation to each of these ligands. Nonlinear curve-fitting was performed for each dose response dataset using GraphPad Prism 6. Measurements were taken from distinct samples.

Characterization of D2 conformations by fluorescence spectroscopy. Following a previously described approach to measure local conformational shifts in the prototypical GPCR B2 (ref. [39]), the monobromobimane fluorescent probe was conjugated to D2 variants via cysteine thiol conjugation. D2 variants were modified to remove exposed cysteine residues close to or inside loop regions (C20A.C132S.C272S.C281S) (note that C272S and C281S are in ICL3, which was not modeled, and therefore follow the gene numbering: measurements were taken from distinct samples) as well as add a cysteine residue to the intracellular helical tips of either TMH6 (Q188C) or TMH5 (L180C) for site specific labeling. Controls were performed to verify that these modified receptors bound ligands and activated Gi2 as the original ones. Receptor variants were expressed and purified as described above. Affinity purified receptor variants were mixed with monobromobimane at the same molarity and incubated on ice for 4–8 h in the dark. The fluorophore-labeled receptor was separated from unconjugated bimane using a desalting column (HiTrap, GE Health Sciences). Monobromobimane conjugated receptors were incubated with various ligands and effectors (4 uM Gi2 and/or 1 µM norapomorphine and/or 1 µM spiperone) for 15 min at room temperature. Residual GTP and GDP in all reaction mixtures were hydrolyzed with apyrase (25 U ml^{-1}). Receptor concentrations were ~2 nM per sample. The fluorescence spectrum was measured on Molecular Devices Flexstation3 plate reader with excitation at 370 nm and emission measured from 420–530 nm at 1 s nm^{-1}. The peaks of maximal fluorescence intensities for various D2 variants and conditions were compared using unpaired two-sided *t*-tests calculated with the GraphPad Prism software.

Relationship between fluorescence spectra and local active conformations occupancy. The following model provides the rationale explaining why ligand binding to a designed receptor results in reduced spectral changes compared to WT if the designed microswitches partially mimic the ligand effects on receptor structure and activity (Fig. 3). Such effects can be formally expressed as follows:

Let us define ΔS^{L}_{WT} as the change in maximal spectrum intensity due to structural change of the WT receptor reaching 100% active state conformation occupancy on ligand agonist binding.

$$\Delta S^{L}_{WT} = S_{WT} - S^{L}_{WT} \quad (1)$$

with S_{WT} and S^{L}_{WT}, the maximal spectrum intensities of the ligand-free and ligand-bound WT receptors, respectively.

If designed mutations shift the receptor toward X% active state conformation occupancy ($X < 100$) by partially mimicking the effects of ligand binding, this will result in the corresponding spectral shift:

$$\Delta S_{DES} = S_{DES} - S_{WT} \quad (2)$$

with S_{DES} and S_{WT} being the maximal spectrum intensities of the ligand-free designed and WT receptors, respectively. Since the designed mutations only partially mimic ligand binding effects, $0 < \Delta S_{DES} < \Delta S^{L}_{WT}$.

If ligand binding further shifts the designed receptor toward 100% active state conformation occupancy,

$$\Delta S^{L}_{DES} = S_{DES} - S^{L}_{DES} \quad (3)$$

with S_{DES} and S^{L}_{DES} being the maximal spectrum intensities of the ligand-free and ligand-bound designed receptors, respectively.

Since both ligand-bound WT and designed receptors reach 100% active state conformation occupancy, $S^{L}_{DES} = S^{L}_{WT}$, then ΔS^{L}_{DES} can be expressed using equations (1) and (2):

$$\Delta S^{L}_{DES} = \Delta S_{DES} + \Delta S^{L}_{WT} \quad (4)$$

Since $\Delta S_{DES} > 0$, $\Delta S^{L}_{DES} < \Delta S^{L}_{WT}$, which demonstrates that, if a designed mutation mimics ligand binding, then ligand binding to that designed receptor will result in a smaller spectral change compared to that observed for the WT.

Homology modeling of D2 WT inactive and active conformations. *Modeling of the D2 WT ligand-free inactive and active conformations.* The closest structurally characterized homologs available were used as templates to model the inactive and active state conformational ensembles adopted by the D2 WT sequence isoform 1 of D2 (http://www.uniprot.org/uniprot/P14416.fasta). The inactive state conformations were modeled starting from the X-ray structure of the antagonist bound dopamine D3 receptor (DRD3, PDB 3PBL) sharing 48% sequence identity with D2. The active state conformations were modeled from the active state GPCR structures of two distant homologs: opsin (23% sequence identity with D2) bound to Gt (PDB 3CAP, 3DQB) and B2 (26% sequence identity with D2) in complex with ligand agonist and heterotrimeric Gs (PDB 3SN6). Models of D2 inactive and active states were generated without bound ligand or G protein using the homology mode of RosettaMembrane as described in ref. [28]. From the above-mentioned simulations, ensembles of low energy models were clustered and centers of the most populated clusters were selected as templates for each ligand-free state (R and R*, see Fig. 1b) in the design calculations of stability microswitches. Specifically, two inactive and six active state models of D2 WT were selected.

Modeling of the D2 WT ligand-bound inactive and active conformations. Ligand-bound D2 models (for example, AR and AR*, see Fig. 1b) were generated by performing ligand docking simulations onto the selected inactive and active state ligand-free D2 models obtained as described above. Specifically, ligands were docked onto D2 models as follows.

The ligand conformer libraries were generated using Omega (OpenEye Inc.) with default parameters from Rosetta's automatic RosettaLigand setup (for example, ewindow 10.0; rms 0.5; Rosetta v.3.2). Ligand docking was performed using a combination of Monte Carlo moves, sidechain repacking and gradient-based minimization with the Rosetta all-atom potential developed for protein–ligand docking. Receptor backbone and sidechain torsions along with ligand torsions, position and orientation were optimized simultaneously[27,48]. All ligand-bound receptor models for a given state (that is, inactive or active) were gathered together and the 5% lowest-energy models were selected and ranked based on the binding energy with the ligand. The selected ligand-bound models were then clustered based on structural similarity of the bound ligand conformation. The representative model of the largest cluster was selected corresponding to the ligand-bound model of the D2 receptor in a given state; that is, ligand-bound D2 inactive and ligand-bound D2 active state conformations.

Modeling of the ligand-free conformations of the D2 local region designed variants. To model the apo conformations (that is, in the absence of ligand and Gi) adopted by D2 variants designed in local regions (Supplementary Fig. 4), we extensively relaxed fully inactive and active conformations of the designed receptors. We used a structure relaxation protocol that samples all backbone and sidechain degrees of freedom without constraints enabling the polypeptide chain to explore an unrestricted conformational space. This protocol allows each designed local region to identify the lowest-energy conformations even if it involves significant conformational changes from the starting template structure. Around 10,000 independent simulations were performed for each variant. The 10% lowest-energy structures were clustered and the center structure of the largest family of structures was selected as the representative model in Supplementary Fig. 4.

Computational design of microswitches. For computational design of stability microswitches perturbing the apo (ligand-free) equilibrium, see the Supplementary Note.

For computational design of allosteric microswitches perturbing structural couplings, see the Supplementary Note.

Qualitative prediction accuracy for designed D2 receptors. *Apo equilibrium shifts.* To calculate the percentage of successfully predicted mutations, we adopted the following criteria. Designed variants predicted to shift the apo equilibrium ($\Delta\Delta G_{apo}$) toward the active state by more than two Rosetta Units were defined successful if they displayed higher constitutive activity than WT by more than two-fold (see Supplementary Fig. 8 and Tables 1 and 2).

Allosteric coupling shifts. To calculate the percentage of successfully predicted mutations, we adopted the following criteria. We gathered measured mutational effects on ligand-induced signaling responses into three categories: enhanced response (that is, gain of function) if ligand efficacy and/or potency were significantly increased from WT; similar response (that is, neutral) if ligand efficacy and/or potency were not significantly altered from WT; weakened response (that is, loss of function) if ligand efficacy and/or potency were significantly decreased from WT. On the prediction side, we gathered calculated mutational effects on the allosteric coupling into three categories: enhanced coupling (that is, gain of function) if the total change in dynamic couplings calculated by NMA according to equation (6 from the Supplementary Note) ($\Delta G^{C}_{DES} - \Delta G^{C}_{WT}$, see Supplementary Note) were >0.25; similar coupling (that is, neutral) if the total change in dynamic couplings were within |0.25|; weakened coupling (that is, loss of function) if the total change in dynamic couplings were <−0.25. A prediction was defined successful if the class of effect on the predicted allosteric coupling matched the class of effect on the measured ligand efficacy and potency.

Quantitative relationship between predictions and experiments for both designed D2 receptors and benchmark of known GPCR mutations. *Apo equilibrium shifts.* As described in Supplementary Fig. 1, the ATSM provides a mathematical framework for relating the calculated energetic and dynamic properties of the designed receptors to the measured allosteric activities (Supplementary Figs. 9 and 10). Without ligand stimulus, the constitutive activity (CA in equation (5)) is directly related to the fraction of ligand-free active state receptor ($f(R^*)$) in the active state, which can be calculated from the equilibrium constant of the ligand-free receptor in the inactive and active state K_R and therefore from the free energy difference between both states ΔG_{apo} by solving the following equations:

$$CA = K_R/(1 + K_R) \quad (5)$$

$$\Delta G_{apo} = -RT \ln(CA/(1 - CA)) \quad (6)$$

However, since Rosetta energies cannot be rigorously converted into physical free energies in kcal per mol, we cannot precisely calculate K_R and the Boltzmann distribution $f(R^*)$ from our calculated energy differences. To circumvent that problem, one could in principle fit the data using equation (6) describing the exact Boltzmann distribution model but with a free parameter in lieu of the energy scaling factor RT. However, as shown in Supplementary Fig. 11, datasets covering a large range of constitutive activities (for example, from 5 to 95% of the maximal receptor activity) are necessary to reliably fit the Boltzmann distribution model but none of our GPCR mutant datasets cover such range in activities (see Supplementary Figs. 9 and 10). Fortunately, as shown in Supplementary Fig. 11, the relationship between constitutive activity and $\Delta\Delta G_{apo}$ is quasi-linear within the range of measured receptor activities. To a first approximation, such a linear relationship enables a direct quantitative comparison between experimental activities and $\Delta\Delta G_{apo}$ energies that is independent of the energy units.

Allosteric coupling shifts. As described in Supplementary Fig. 1, the ATSM relates the allosteric coupling α to the ligand potency EC_{50} as follows:

$$EC_{50} = (1 + K_R)/K_A(1 + \alpha K_R) \quad (7)$$

with K_A being the intrinsic receptor ligand affinity. Our ligand docking simulations and receptor energy calculations indicate that the WT and receptors designed with altered allosteric ligand responses have very similar K_A and K_R. Therefore, the ratio between EC_{50} between two receptor variants X and Y simplifies to:

$$EC_{50X}/EC_{50Y} = (1 + \alpha_Y K_{RY})/(1 + \alpha_X K_{RX}) \quad (8)$$

Since $\alpha K_R \gg 1$ for a full agonist such as dopamine[13], equation (8) simplifies to:

$$EC_{50X}/EC_{50Y} = \alpha_Y/\alpha_X \quad (9)$$

Then equation (6 from the Supplementary Note) can be rewritten as follows:

$$RT(pEC_{50X} - pEC_{50Y}) = -RT\log(\alpha_X/\alpha_Y) = \Delta\Delta G^{C} \quad (10)$$

Therefore, we expect a linear relationship between changes in structural coupling $\Delta\Delta G^C$ and changes in ligand potency EC_{50}. $\Delta\Delta G^C$ are the changes in dynamic couplings calculated by NMA as described above.

Benchmark of known mutational effects on receptor signaling activities. Delta opioid, rhodopsin, dopamine and B2 receptors were selected for the benchmark because large experimental datasets generated with consistent experimental methods were available for these receptors[43,44,49–53].

The following criteria were applied to select the datasets and mutations. Only mutations of residues in the TMH region or helix 8 were considered to focus on long-range allosteric effects and avoid mutations that may directly affect ligand or G protein binding. Mutations involving proline residues were not considered as they often disrupt TMH structures. For the prediction of allosteric effects affecting ligand potency, mutations inducing large effects on constitutive activities were not considered since equation (10) relating directly EC_{50} shifts to allosteric coupling shifts would not be valid.

Since the fully induced activities were not available for all mutant receptors, constitutive activities were normalized to the fully induced WT activity (at saturating ligand concentration with a full agonist). We further normalized given activities based on receptor expression (either receptor cell surface expression or total expression), where such data were available[43,50]. Activity data for rhodopsin mutations were not normalized.

Our benchmark totalizes 109 mutations across four different receptors (D2, B2, delta opioid receptor, rhodopsin) that involves mutations at 40 unique sites and 26 unique combinations of sites.

Available X-ray structures were used for modeling the inactive and active states of opsin (3DQB, 3C9L) and B2 (3SN6, 2RH1) and for modeling the inactive state of the delta opioid receptor (4N6H). Homology models were generated for the dopamine receptor and for the active state of the delta opioid receptor as described above. Ligand-free receptor energies and long-range couplings were calculated as described above for the designed receptors; that is, by RosettaMembrane and NMA, respectively.

Reporting Summary. Further information on research design is available in the Nature Research Reporting Summary linked to this article.

Data availability

The data that support the findings of this study are available from the corresponding author upon reasonable request.

Code availability

Protein modeling and design applications (IPHoLD, RosettaMembrane) are available in the latest version of the Rosetta software package (https://www.rosettacommons.org/software) or at https://doi.org/10.5281/zenodo.3460811. Bio3D is available at: http://thegrantlab.org/bio3d/index.php.

References

44. Han, M., Smith, S. O. & Sakmar, T. P. Constitutive activation of opsin by mutation of methionine 257 on transmembrane helix 6. *Biochemistry* **37**, 8253–8261 (1998).
45. Graber, S. G., Figler, R. A. & Garrison, J. C. Expression and purification of functional G protein alpha subunits using a baculovirus expression system. *J. Biol. Chem.* **267**, 1271–1278 (1992).
46. Miller, M. et al. in *TRP Channels* (ed. Zhu, M. X.) 1–20 (Boca Raton, FL, CRC Press/Taylor & Francis, 2011).
47. Young, M. et al. Computational design of orthogonal membrane receptor-effector switches for rewiring signaling pathways. *Proc. Natl Acad. Sci. USA* **115**, 7051–7056 (2018).
48. Davis, I. W. & Baker, D. RosettaLigand docking with full ligand and receptor flexibility. *J. Mol. Biol.* **385**, 381–392 (2009).
49. Befort, K., Zilliox, C., Filliol, D., Yue, S. & Kieffer, B. L. Constitutive activation of the delta opioid receptor by mutations in transmembrane domains III and VII. *J. Biol. Chem.* **274**, 18574–18581 (1999).
50. Cavalli, A., Babey, A. M. & Loh, H. H. Altered adenylyl cyclase responsiveness subsequent to point mutations of Asp 128 in the third transmembrane domain of the delta-opioid receptor. *Neuroscience* **93**, 1025–1031 (1999).
51. Decaillot, F. M. et al. Opioid receptor random mutagenesis reveals a mechanism for G protein-coupled receptor activation. *Nat. Struct. Biol.* **10**, 629–636 (2003).
52. Han, M., Lin, S. W., Minkova, M., Smith, S. O. & Sakmar, T. P. Functional interaction of transmembrane helices 3 and 6 in rhodopsin. Replacement of phenylalanine 261 by alanine causes reversion of phenotype of a glycine 121 replacement mutant. *J. Biol. Chem.* **271**, 32337–32342 (1996).
53. Han, M., Lin, S. W., Smith, S. O. & Sakmar, T. P. The effects of amino acid replacements of glycine 121 on transmembrane helix 3 of rhodopsin. *J. Biol. Chem.* **271**, 32330–32336 (1996).

Acknowledgements

We thank R. Sharma for setting up some NMA calculations, T. Wensel and his laboratory for sharing experimental protocols and members of the Barth laboratory for helpful discussion. This work was supported by funding from EPFL and the Ludwig Institute for Cancer Research, partially supported by a grant from the National Institute of Health (no. 1R01GM097207), and by a supercomputer allocation from XSEDE (no. MCB120101) to P.B.

Author contributions

P.B. designed the studies. P.B., K.-Y.M.C. and D.K. performed the calculations. K.-Y.M.C. and D.K. performed experiments on D2. P.B., D.K. and K.-Y.M.C. analyzed the data. P.B. wrote the manuscript.

Competing interests

P.B. declares the following patent application: patent applicant, Ecole Polytechnique Fédérale de Lausanne. Name of inventor(s), Patrick Barth. Application number, EP 19189259.5. Status of application, priority year. Specific aspect of manuscript covered in patent application, methods and protein variants.

Additional information

Supplementary information is available for this paper at https://doi.org/10.1038/s41589-019-0407-2.

Correspondence and requests for materials should be addressed to P.B.

Reprints and permissions information is available at www.nature.com/reprints.

nature research

Corresponding author(s): Patrick Barth

Reporting Summary

Nature Research wishes to improve the reproducibility of the work that we publish. This form provides structure for consistency and transparency in reporting. For further information on Nature Research policies, see Authors & Referees and the Editorial Policy Checklist.

Statistical parameters

When statistical analyses are reported, confirm that the following items are present in the relevant location (e.g. figure legend, table legend, main text, or Methods section).

n/a	Confirmed	
☐	☒	The exact sample size (*n*) for each experimental group/condition, given as a discrete number and unit of measurement
☐	☒	An indication of whether measurements were taken from distinct samples or whether the same sample was measured repeatedly
☐	☒	The statistical test(s) used AND whether they are one- or two-sided *Only common tests should be described solely by name; describe more complex techniques in the Methods section.*
☒	☐	A description of all covariates tested
☒	☐	A description of any assumptions or corrections, such as tests of normality and adjustment for multiple comparisons
☐	☒	A full description of the statistics including central tendency (e.g. means) or other basic estimates (e.g. regression coefficient) AND variation (e.g. standard deviation) or associated estimates of uncertainty (e.g. confidence intervals)
☒	☐	For null hypothesis testing, the test statistic (e.g. *F*, *t*, *r*) with confidence intervals, effect sizes, degrees of freedom and *P* value noted *Give P values as exact values whenever suitable.*
☒	☐	For Bayesian analysis, information on the choice of priors and Markov chain Monte Carlo settings
☒	☐	For hierarchical and complex designs, identification of the appropriate level for tests and full reporting of outcomes
☒	☐	Estimates of effect sizes (e.g. Cohen's *d*, Pearson's *r*), indicating how they were calculated
☐	☒	Clearly defined error bars *State explicitly what error bars represent (e.g. SD, SE, CI)*

Our web collection on statistics for biologists may be useful.

Software and code

Policy information about availability of computer code

Data collection	Experimental data were obtained with the software Softmax Pro 7, provided by Molecular Devices. Computational data were generated using protein modeling and design applications (IPHoLD, RosettaMembrane) available in the latest version of the Rosetta software package (https://www.rosettacommons.org/software) or at https://doi.org/10.5281/zenodo.3460811, as well as Bio3D available at: http://thegrantlab.org/bio3d/index.php
Data analysis	Experimental data were analyzed using the Graphpad Prism 6 software. ImageJ version 1.52A was used to determine western blot band relative intensities.

For manuscripts utilizing custom algorithms or software that are central to the research but not yet described in published literature, software must be made available to editors/reviewers upon request. We strongly encourage code deposition in a community repository (e.g. GitHub). See the Nature Research guidelines for submitting code & software for further information.

Data

Policy information about availability of data

All manuscripts must include a data availability statement. This statement should provide the following information, where applicable:

- Accession codes, unique identifiers, or web links for publicly available datasets
- A list of figures that have associated raw data
- A description of any restrictions on data availability

The data that support the findings of this study are available from the corresponding author upon reasonable request.

Field-specific reporting

Please select the best fit for your research. If you are not sure, read the appropriate sections before making your selection.

☒ Life sciences ☐ Behavioural & social sciences ☐ Ecological, evolutionary & environmental sciences

For a reference copy of the document with all sections, see nature.com/authors/policies/ReportingSummary-flat.pdf

Life sciences study design

All studies must disclose on these points even when the disclosure is negative.

Sample size	The standard N=3 replicates were used for each experiment typically, which is the standard in similar studies. No samples size calculations were performed.
Data exclusions	Receptor activity data were excluded from use if the determined difference in surface expression was greater than 10% from that of the wildtype receptor. This criteria was pre-established to ensure robust receptor variant activity comparison without the need to normalize based on receptor surface expression. In the benchmark, mutations affecting directly ligand and G-protein binding were excluded. This criteria was pre-established to focus the analysis on long-range allosteric effects. In the benchmark, mutations involving proline residues were not considered. This criteria was pre-established because proline residues are known to considerably destabilize and distort transmembrane helices and these effects are very challenging to predict accurately.
Replication	To verify the reproducibility of the experiments, we performed the standard sample size replicates and we found that all replication attempts were successful.
Randomization	Randomization of groups/samples is not relevant to our study as no human or animal subjects were used.
Blinding	All design calculations were performed blindly without prior knowledge of experimental outcomes, and experiments were performed to validate the calculations. Benchmark calculations were performed as in blind predictions and the results were not biased by the knowledge of known mutational effects.

Reporting for specific materials, systems and methods

Materials & experimental systems

n/a	Involved in the study
☐	☒ Unique biological materials
☐	☒ Antibodies
☐	☒ Eukaryotic cell lines
☒	☐ Palaeontology
☒	☐ Animals and other organisms
☒	☐ Human research participants

Methods

n/a	Involved in the study
☒	☐ ChIP-seq
☒	☐ Flow cytometry
☒	☐ MRI-based neuroimaging

Unique biological materials

Policy information about availability of materials

Obtaining unique materials	All unique materials (variants of the dopamine D2 receptor in pcDNA3.1+ vector) are readily available. The HA-tagged D2 WT construct was purchased from cdna.org (catalog no.: DRD010TN00). Derived mutations were created by subjecting said WT

construct to site-directed mutagenesis, followed by confirmation of desired mutation by sequencing.

Antibodies

Antibodies used	anti-HA mouse monoclonal antibody, clone 2-2.2.14, Fisher Scientific cat. no.: 26183, lot UB278416, dilution 1:300; Anti-mouse IgG, HRP-linked Antibody from Cell Signaling Technology, cat. no.: 7076, lot 33, dilution 1:2000
Validation	the anti-HA primary (mouse) antibody is validated by the manufacturer, ThermoFisher Scientific, as stated on their website: https://www.thermofisher.com/ch/en/home/life-science/antibodies/invitrogen-antibody-validation.html Certificate of analysis for the used lot can be found here: https://assets.thermofisher.com/TFS-Assets/LSG/certificate/Certificates-of-Analysis/26183_UB278416.PDF

Eukaryotic cell lines

Policy information about cell lines

Cell line source(s)	HEK293T from Ted Wensel at Baylor College of Medicine; HEK293 cells stably expressing the TRPC4B ion channel, from the Lab of Michael Xu at UT Houston.
Authentication	HEK293 with TrpC4beta was selected for stable expression via G418 and screened for TrpC4beta expression with western blots. HEK293T cells were visually inspected for cell morphologies that are consistent with previous morphological examinations of the cell lines. No further authentication was performed.
Mycoplasma contamination	The used cell lines tested negative for the presence of mycoplasma. Mycoplasma detection was performed by qPCR against several mycoplasma species-specific sequences.
Commonly misidentified lines (See ICLAC register)	No commonly misidentified cell lines were used in this study.